JMEMS Letters

Tunable Fabry-Perot Filter Using Hybrid Integrated Grating and Slot Microstructures

Yu-Sheng Lin and Chengkuo Lee, *Member, IEEE*

***Abstract*— The design, fabrication, and characterization of an electrostatically tunable optical Fabry–Perot (FP) filter with hybrid integration of grating and slot structures are presented. Using deep reactive ion etching, antireflection grating (ARG) structures are created at the inner wall of the FP resonator to enhance the performance of a tunable FP filter. The moving parts are released by etching the buried oxide layer using hydrofluoric acid vapor. The optical tuning range of the device is 19 nm. Attributed to the ARG structures, the light propagates effectively through the FP resonator. Thus, the *Q*-factor of the resonant peak is enhanced more than threefold when an FP resonator with ARG structures is compared with an FP resonator using one-slot (Si/air/Si) structure. With the optimized design, an FP resonator comprising of the ARG and two-slot structures shows record-breaking *Q*-factor, i.e., 9762. [2014-0081]**

***Index Terms*— CMOS compatible, microelectromechanical systems (MEMS), tunable Fabry-Perot (FP) filter, grating structures.**

I. Introduction

Recently, the optical microelectromechanical systems (MEMS) technology have been used to demonstrate optical switch, variable optical attenuator (VOA), laser, and filter in out-of-plane configurations [1], [2], and similar devices in in-plane configurations with advantages of fiber alignment applications [3]. In addition to the optical communication related applications, recent research interests have been moved to chemical analysis, biomedical imaging, and various sensors systems [4]. All of these systems require a filtering device that is small in size, consumes low power, and is operable at high speed. The tunable fiber-optic filter is getting attention as a useful filtering device for those applications. Fabry-Perot (FP) cavity is a typical structure of the optical filters, which consists of two parallel distributed Bragg reflectors (DBR) separated by a gap. FP filters have also been enabling optical devices with wavelength selective properties in optical communication systems, which demand narrow full width at half maximum (FWHM), wide free spectrum range (FSR) and wide dynamic range. Based on the MEMS technology, the FP tunable filter can not only be miniaturized but also be fabricated with merits of high tuning speed, low insertion loss, low driving voltage, and batch fabrication, etc. In most of above-mentioned applications, the system performance is proven to be mainly dependent on the quality factor (Q-factor) and the finesse (F) of the FP response.

Until now, the Q-factor of tunable FP filter with planar Bragg mirrors is mostly limited to a few hundreds [4]–[6]. To enhance the Q-factor and F of a linear configured FP filter, waveguide-based FP filters [7], [8], photonics crystal resonators [9], or ring resonators [10], [11] are often considered. However, the coupling to radiation modes in integrated optical structures, intrinsic absorption in the materials, and scattering on structural surface will result in the propagation losses in these above methods [12].

For FP filter based on free space scheme, the light propagating through the Si/air DBR mirrors suffers serious reflection because of the high refractive index (RI) contrast between Si and air. Furthermore, the Gaussian beam divergence and surface roughness of mirror are dominant sources of loss, which are difficult to prevent in the processing and testing [13]. Therefore, our previous results proposed the antireflection grating (ARG) structures on the inner walls of the FP resonator to allow the light resonate effectively in the FP cavity and propagate through the resonators, hence enhancing the performance of the optical filter in the mid-infrared wavelength [14]. In this letter, to optimize the tunable high-Q FP filters using hybrid integration of the triangular grating (TG) and slot structures based on Si/air DBR mirrors in the C-band, we investigate four different configurations including tunable FP filters with one slot, TG, hybrid integration of the TG and one slot, hybrid integration of the TG and two slots, respectively, where configurations are denoted as "S-1", "TG-1", "TG-2", and "TG-3", respectively.

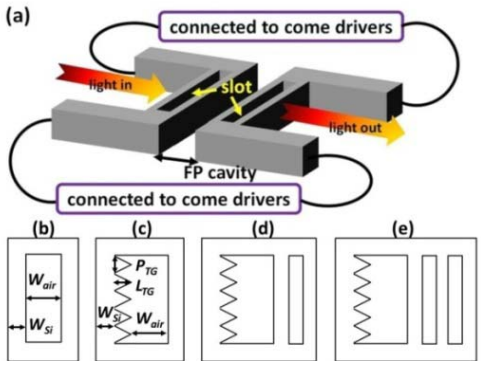

Fig. 1. Schematic drawings of (a) S-1 integrated with comb drive actuators; (b-e) are S-1, TG-1, TG-2, and TG-3 configurations, respectively.

II. Design and Fabrication

Figure 1(a) shows schematic drawing of the typical design of a tunable FP resonator, including Si/air/Si slabs with $P = 1.5$ periods being actuated by comb drive actuators. In order to compare designs with top views of S-1, TG-1, TG-2, and TG-3 configurations are shown in Fig. 1 (b-e), respectively. The basic principle of grating structures on the sidewall of resonator lies in the RI of the surface layer varying gradually from air to substrate, and thus effectively suppresses the specular reflectance at the interface of the two media [15]. The design of Si/air DBR can be used

Manuscript received March 12, 2014; revised May 5, 2014; accepted May 7, 2014. Date of publication July 10, 2014; date of current version September 29, 2014. This work was supported by the National University of Singapore, Singapore, through the Ministry Of Education (MOE) Academic Research Fund under Grant Tier 2-MOE2012-T2-2-154. Subject Editor H. Zappe.

The authors are with the Department of Electrical and Computer Engineering, National University of Singapore, Singapore 117576 (e-mail: elelinys@nus.edu.sg; elelc@nus.edu.sg).

Color versions of one or more of the figures in this letter are available online at http://ieeexplore.ieee.org.

Digital Object Identifier 10.1109/JMEMS.2014.2322870

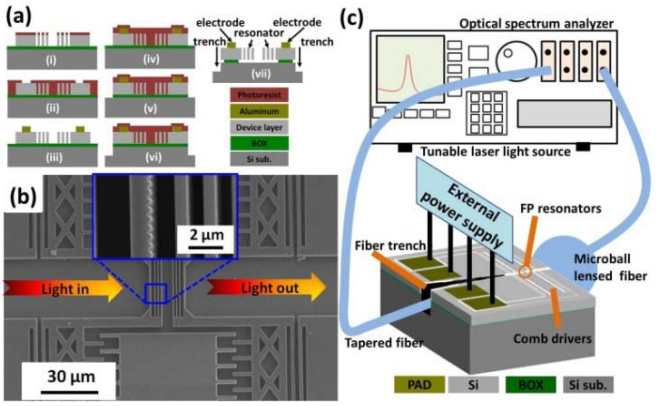

Fig. 2. (a) The fabrication process flow of in-plane FP filter. (b) SEM image of in-plane FP filter with TG-3 actuated by comb drivers. The inset shows the zoom-in SEM image of blue square. (c) Schematic diagram of the optical testing setup with a sharp conical fiber and a microball lensed fiber used for light coupling to and from the device.

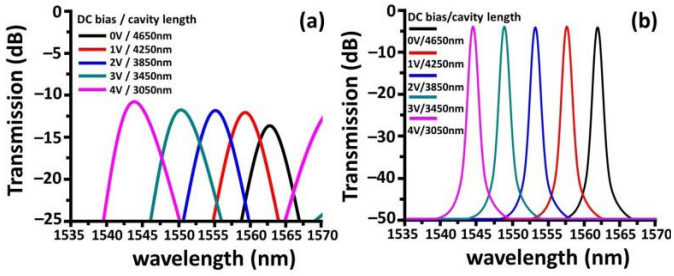

Fig. 3. Experimental results of (a) S-1 and (b) TG-1, respectively.

$W_{eff} = m \cdot \lambda_0/4 \cdot n_{eff}$ to calculate the widths of Si slab and air slot, where λ_0, n_{eff}, and m are wavelength in free space, effective RI and an integer, respectively. Here, the width of Si slab (W_{Si}) and air slot (W_{air}) are 1114 nm and 1163 nm, respectively, where $\lambda_{center} = 1550$ nm and $n_{eff} = 3.477$. The feature sizes of TG period (P_{TG}) and length (L_{TG}) are 500 nm and 420 nm, respectively.

Figure 2(a) shows the CMOS compatible micro fabrication process flow of in-plane tunable FP filter. A n-type (100) SOI wafer with 5 μm thick Si device layer, 1 μm thick buried oxide (BOX) layer and 650 μm Si handle layer was used as the starting material. Firstly, the features of the microstructures such as the FP resonators and electrostatic comb drive actuators were defined by using deep reactive ion etching (DRIE). Secondly, the aluminum (Al) electrodes were deposited and patterned by using lift-off process. Thirdly, the 1 μm thick BOX layer was patterned and etched down to Si substrate, and then the Si substrate was etched 60 μm in depth for fiber trench. Finally, the freestanding structures were then achieved by utilizing hydrofluoric acid vapor to etch away the buried oxide layer below the FP resonators and comb drive actuator structures. We illustrate the proposed device in Fig. 2(b), as seen in the scanning electron micrograph (SEM) of TG-3 configuration. The optical testing setup is shown in Fig. 2(c). The devices were tested using a tunable laser in wavelength ranging from 1520 to 1620 nm. Single mode SMF-28 with tapered fiber with conical tip of 2 μm in diameter was inserted into fiber trench to provide the input light toward FP resonator. A microball lensed fiber with 300 μm in diameter was placed close to edge of silicon chip on the output port side and deployed to collect the spectral response on the end of device, respectively. The dc bias was applied to the comb drive actuators by an external power supply in order to adjust the length of FP cavity.

III. Results and Discussion

Figure 3 shows the experimental results of S-1 and TG-1 configurations, respectively. The device was tested for a wavelength range of 35 nm starting from 1535 nm to 1570 nm at different bias voltages with a wavelength step of 0.5 nm. The voltage was swept from 0 V to 4 V with an increment of 1 V. This result shows the FP spectra when cavity length is shrunk by 400 nm per step with actuation of the double-side comb drivers. It is clear observed that the wavelength blue shifts from higher value to lower value due to the decrease in the resonant cavity length as the two FP resonators move toward each other under actuation. The wavelength shift, $\Delta\lambda$, as a function of voltage and the response time of tuning can be expressed by [16],

$$\Delta\lambda \approx \frac{n_0 \cdot \varepsilon_0 \cdot A}{k \cdot m \cdot g^2} \Delta V_{bias}^2 = \frac{n_0 \cdot \varepsilon_0 \cdot A \cdot (2\pi f V_a \Delta t)^2}{k \cdot m \cdot g^2} \quad (1)$$

where ε_0 and n_0, are the permittivity and RI in free-space, respectively, A is the area of the comb driver, g is gap of comb finger, k is the spring constant of comb driver, V_a is the amplitude of input signal and f is a variable frequency. The performance of a tunable FP filter is characterized by its Q-factor and F which are expressed as

$$Q = \frac{\lambda}{FWHM} = \frac{\lambda_0 F(R)}{FSR} = \frac{\lambda_0 \pi \sqrt{R(\lambda)}}{FSR[1 - R(\lambda)]} \quad (2)$$

where $R(\lambda)$ is the wavelength dependent reflectivity, and FWHM means full width at half maximum intensity. The FWHM of spectra of these two types of tunable FP filters are 5.98 nm (S-1) and 2.00 nm (TG-1), respectively. Q-factors and F, calculated using equation (2), for these two tunable FP filters are 261 (S-1) and 781 (TG-1) for Q-factors, 7.77 (S-1) and 23.25 (TG-1) for F, respectively. This optical performance improvement can be attributed to the ARG structures superimposed on the FP resonator. The reflectance of propagation light is expressed by equation (3), where n_0 is RI of air ($n_0 = 1$), n_s is RI of Si ($n_s = 3.477$), and n_{eff} is effective RI of ARG ($n_{eff} = \sqrt{(AB + n_s^2)/2A}$), where $A = f + (1 - f)n_s^2$, $B = 1 - f + fn_s^2$ and f is the filling factor of the ARG structures, which is the volume percentage of the ARG structures in the FP resonator. The uniqueness of effective medium approximation is that it can be extended to multiple numbers of constituent layers expressed by equation (4) [17]. The role of ARG, therefore, is to increase the amount of light being transmitted to the DBR mirrors and resonating in the FP cavities.

$$R = 1 - \frac{4n_0 n_s n_{eff}^2}{(n_0 n_s + n_{eff}^2)^2} = \left[\frac{n_0 n_s - n_{eff}^2}{n_0 n_s + n_{eff}^2}\right]^2 \quad (3)$$

$$\sum_{i=1}^{N} f_i \left[\frac{2An_i^2 - AB + n_s^2}{2An_i^2 + 2(AB + n_s^2)}\right] = 0 \quad (4)$$

The results in Fig. 3 have shown that the optical performance of TG-1 is better than that of S-1. In this consideration, we further optimized the performance of tunable FP filter by using more periods of Si/air DBR mirrors, i.e., TG-2 and TG-3, with the cost of reduced optical intensity. Figure 4(a) compares the experimentally measured results of TG-1, TG-2, and TG-3, respectively. The corresponding SEM images of FP resonators of Fig. 4(a) are shown in Fig. 4(c-e), respectively. Using equation (2), Q-factors of these devices are derived as 781, 1950, and 3122 for FP filter with TG-1, TG-2, and TG-3, respectively. The performance of TG-2 is 7.5-fold and 2.5-fold higher than that of S-1 and TG-1, respectively. The Q-factor is enhanced 1.6-fold when TG-3 is compared with that of TG-2. On the other hand, M. Malak et al. reported Q-factor of

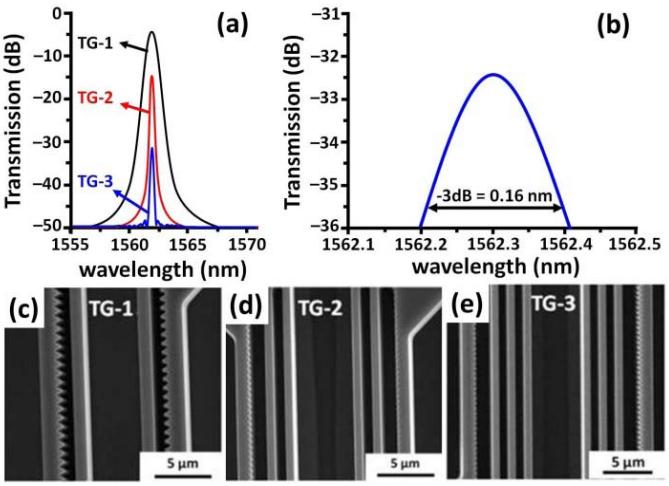

Fig. 4. (a) Experimental results of TG-1, TG-2, and TG-3, respectively. (b) The FWHM of TG-3 is 0.16 nm leading to a Q-factor of 9762 calculated at −3dB. (c-e) SEM images of FP resonators of TG-1, TG-2, and TG-3, respectively.

8818 measured at −3dB from maximum intensity for multilayered silicon-air Bragg mirrors of cylindrical shape [18]. Considering the same definition of Q-factor measured at −3dB intensity, the measured FWHM of TG-3 at −3dB is 0.16 nm which leads to a Q-factor of 9762 as shown in Fig. 4(b). This value is obtained for TG-3 with grating structures per mirror and a physical cavity length of 4650 nm. This result shows 11% improvement in comparison to the Q-factor of 8818 [18]. The improved Q-factor is mainly attributed to the gradient RI on the sidewalls of the FP resonator. It helps the light resonated in the FP cavity and propagated through the resonator effectively, resulting in a narrower FWHM.

IV. Conclusion

We demonstrated a low-voltage electrostatically tunable optical FP filter integrated with ARG structures. The optical tuning range is 19 nm achieved by giving 4 volts bias to the comb drive actuator. Such integration of ARG structures into tunable FP filters can enhance their optical performance due to the gradient RI on the sidewalls of the FP resonator. In the case for Q-factor, TG-3 was enhanced 12-fold and 4-fold better than those values of S-1 and TG-1, respectively. These tunable FP filters show attractive features for potential applications in optical fiber communication, optical fiber sensing, spectrum analysis and fiber laser, etc.

References

[1] K. H. Koh, B. W. Soon, J. M.-L. Tsai, A. J. Danner, and C. Lee, "Study of hybrid driven micromirrors for 3-D variable optical attenuator applications," *Opt. Exp.*, vol. 20, no. 19, pp. 21598–21611, 2012.

[2] C. P. Ho, P. Pitchappa, P. Kropelnicki, J. Wang, Y. Gu, and C. Lee, "Development of polycrystalline silicon based photonic crystal membrane for mid-infrared applications," *IEEE J. Sel. Topics Quantum Electron.*, vol. 20, no. 4, p. 4900107, Jul./Aug. 2014.

[3] C. Lee and Y.-S. Lin, "A new micromechanism for transformation of small displacements to large rotations for a VOA," *IEEE Sensors J.*, vol. 4, no. 4, pp. 503–509, Aug. 2004.

[4] R. St-Gelais, J. Masson, and Y.-A. Peter, "All-silicon integrated Fabry–Pérot cavity for volume refractive index measurement in microfluidic systems," *Appl. Phys. Lett.*, vol. 94, no. 24, p. 243905, 2009.

[5] A. Lipson and E. M. Yeatman, "Low-loss one-dimensional photonic bandgap filter in (110) silicon," *Opt. Lett.*, vol. 31, no. 3, pp. 395–397, 2006.

[6] B. Saadany *et al.*, "Free-space tunable and drop optical filters using vertical Bragg mirrors on silicon," *IEEE J. Sel. Topics Quantum Electron.*, vol. 12, no. 6, pp. 1480–1488, Nov./Dec. 2006.

[7] C. A. Barrios, V. R. Almeida, R. R. Panepucci, B. S. Schmidt, and M. Lipson, "Compact silicon tunable Fabry–Pérot resonator with low power consumption," *IEEE Photon. Technol. Lett.*, vol. 16, no. 2, pp. 506–508, Feb. 2004.

[8] M. W. Pruessner, T. H. Stievater, and W. S. Rabinovich, "In-plane microelectromechanical resonator with integrated Fabry–Pérot cavity," *Appl. Phys. Lett.*, vol. 92, no. 8, p. 081101, 2008.

[9] X. Chew, G. Zhou, F. S. Chau, and J. Deng, "Nanomechanically tunable photonic crystal resonators utilizing triple-beam coupled nanocavities," *IEEE Photon. Technol. Lett.*, vol. 23, no. 18, pp. 1310–1312, Sep. 15, 2011.

[10] C.-W. Tseng, C.-W. Tasi, K.-C. Lin, M.-C. Lee, and Y.-J. Chen, "Study of coupling loss on strongly-coupled, ultra compact microring resonators," *Opt. Exp.*, vol. 21, no. 6, pp. 7250–7257, 2013.

[11] W.-Y. Chiu *et al.*, "A photonic crystal ring resonator formed by SOI nano-rods," *Opt. Exp.*, vol. 15, no. 23, pp. 15500–15506, 2007.

[12] M. Lipson, "Guiding, modulating, and emitting light on silicon-challenges and opportunities," *J. Lightw. Technol.*, vol. 23, no. 12, pp. 4222–4238, Dec. 2005.

[13] R. St-Gelais, A. Poulin, and Y.-A. Peter, "Advances in modeling, design, and fabrication of deep-etched multilayer resonators," *J. Lightw. Technol.*, vol. 30, no. 12, pp. 1900–1908, Jun. 15, 2012.

[14] Y. S. Lin, C. P. Ho, K. H. Koh, and C. Lee, "Fabry–Pérot filter using grating structures," *Opt. Lett.*, vol. 38, no. 6, pp. 902–904, 2013.

[15] Y. S. Lin, W. C. Hsu, K. C. Huang, and J. A. Yeh, "Wafer-level fabrication and optical characterization of nanoscale patterned sapphire substrates," *Appl. Surf. Sci.*, vol. 258, no. 1, pp. 2–6, 2011.

[16] Y. Yeh, D. Park, and S. H. Park, "High-speed measurement of free spectral range voltage of tunable filters," *Opt. Lett.*, vol. 34, no. 1, pp. 52–54, 2009.

[17] W. H. Southwell, "Pyramid-array surface-relief structures producing antireflection index matching on optical surfaces," *J. Opt. Soc. Amer. A*, vol. 8, no. 3, pp. 549–553, 1991.

[18] M. Malak, N. Pavy, F. Marty, Y.-A. Peter, A. Q. Liu, and T. Bourouina, "Micromachined Fabry—Pérot resonator combining submillimeter cavity length and high quality factor," *Appl. Phys. Lett.*, vol. 98, no. 21, p. 211113, 2011.